

Spectral Partitioning in Diffraction Tomography

S.K. Lehman, D.H. Chambers, J.V. Candy

This article was submitted to
44th International Symposium on Optical Science, Engineering, and
Instrumentation, Denver, CO, July 18-23, 1999

June 14, 1999

U.S. Department of Energy

Lawrence
Livermore
National
Laboratory

DISCLAIMER

This document was prepared as an account of work sponsored by an agency of the United States Government. Neither the United States Government nor the University of California nor any of their employees, makes any warranty, express or implied, or assumes any legal liability or responsibility for the accuracy, completeness, or usefulness of any information, apparatus, product, or process disclosed, or represents that its use would not infringe privately owned rights. Reference herein to any specific commercial product, process, or service by trade name, trademark, manufacturer, or otherwise, does not necessarily constitute or imply its endorsement, recommendation, or favoring by the United States Government or the University of California. The views and opinions of authors expressed herein do not necessarily state or reflect those of the United States Government or the University of California, and shall not be used for advertising or product endorsement purposes.

This is a preprint of a paper intended for publication in a journal or proceedings. Since changes may be made before publication, this preprint is made available with the understanding that it will not be cited or reproduced without the permission of the author.

This report has been reproduced directly from the best available copy.

Available electronically at <http://www.doe.gov/bridge>

Available for a processing fee to U.S. Department of Energy
and its contractors in paper from
U.S. Department of Energy
Office of Scientific and Technical Information
P.O. Box 62
Oak Ridge, TN 37831-0062
Telephone: (865) 576-8401
Facsimile: (865) 576-5728
E-mail: reports@adonis.osti.gov

Available for the sale to the public from
U.S. Department of Commerce
National Technical Information Service
5285 Port Royal Road
Springfield, VA 22161
Telephone: (800) 553-6847
Facsimile: (703) 605-6900
E-mail: orders@ntis.fedworld.gov
Online ordering: <http://www.ntis.gov/ordering.htm>

OR

Lawrence Livermore National Laboratory
Technical Information Department's Digital Library
<http://www.llnl.gov/tid/Library.html>

Spectral Partitioning In Diffraction Tomography *

Sean K. Lehman, David H. Chambers, and James V. Candy
Lawrence Livermore National Laboratory

ABSTRACT

The scattering mechanism of diffraction tomography is described by the integral form of the Helmholtz equation. The goal of diffraction tomography is to invert this equation in order to reconstruct the object function from the measured scattered fields.

During the forward propagation process, the spatial spectrum of the object under investigation is "smeared," by a convolution in the spectral domain, across the propagating and evanescent regions of the received field. Hence, care must be taken in performing the reconstruction, as the object's spectral information has been moved into regions where it may be considered to be noise rather than useful information. This will reduce the quality and resolution of the reconstruction.

We show how the object's spectrum can be partitioned into resolvable and non-resolvable parts based upon the cutoff between the propagating and evanescent fields. Operating under the Born approximation, we develop a beam-forming on transmit approach to direct the energy into either the propagating or evanescent parts of the spectrum. In this manner, we may individually interrogate the propagating and evanescent regions of the object spectrum.

Keywords: Diffraction Tomography, Evanescent Fields, Beam-Forming

1. INTRODUCTION

Most current diffraction tomography reconstruction techniques have been developed for the far-field, ignoring the near-field phenomenon of evanescent fields. These evanescent fields which decay exponentially as the distance from the scattering object, carry high spatial frequency information. Thus, when operating in the near-field, they can be incorporated into a reconstruction algorithm to achieve higher resolution reconstructions.

There exists a difficulty, however, in the forward scattering process which is described by a convolution in the spectral domain between the object and total field spectra. This convolution results in a "smearing" of the propagating and evanescent spectral components. We propose a method of circumventing this smearing by using a beam-forming transmitting array to direct the energy into the propagating part of the spectrum.

In this paper, we consider the case of a wide-band planar scanning device such as encountered in a ground penetrating radar. We assume near-field operation as in the case of small, shallowly buried land mines, or objects concealed within a wall. In these cases the evanescent fields can be measured.

In the next section, we develop a symbolic, operator notation to represent the forward scattering mechanism. We then use this to show how the object's spectrum is convolved with the total field spectrum. In Section 3, we develop the beam-forming mechanism for isolating spectral components. Finally, in the last section, we show from both simulation and laboratory experiment that when operating in a near-field environment, the evanescent fields consist of approximately 25% of the backscattered energy.

Note: Throughout this work, the volume under investigation lies in the region of $z \geq 0$. The transmit/receive plane is $z = z_0 < 0$. Thus

$$|z - z'| = -(z_0 - z') \quad (1)$$

for reflection mode.

*Work performed under the auspices of U.S. Department of Energy by the Lawrence Livermore National Laboratory under contract No. W-7405-ENG-48

2. SYMBOLIC DEVELOPMENT OF FORWARD SCATTERING PROCESS

2.1. Introduction

We begin with the integral form of the vector Helmholtz equation,¹

$$\mathbf{E}_{scat}(\mathbf{r}_\perp, z_0, \omega) = k_0^2(\omega) \int d\mathbf{r}' \overset{\leftrightarrow}{\mathbf{G}}(\mathbf{r}_\perp - \mathbf{r}'_\perp, z_0 - z', \omega) \cdot \mathbf{E}(\mathbf{r}'_\perp, z', \omega) o(\mathbf{r}'_\perp, z', \omega) \quad (2)$$

where the total field is defined as the sum of the scattered field and the incident field,

$$\mathbf{E}(\mathbf{r}_\perp, z, \omega) \equiv \mathbf{E}_{inc}(\mathbf{r}_\perp, z, \omega) + \mathbf{E}_{scat}(\mathbf{r}_\perp, z, \omega), \quad (3)$$

$o(\mathbf{r}_\perp, z, \omega)$ is the object function to be determined, and $\overset{\leftrightarrow}{\mathbf{G}}(\mathbf{r}_\perp - \mathbf{r}'_\perp, z_0 - z', \omega)$ is the dyadic free-space Green's function. Note: We have explicitly separated the coordinate system into components lying in the measurement plane, \mathbf{r}_\perp , and perpendicular to it, z .

Symbolically, Eqn. 2 is written as

$$\tilde{\mathbf{E}}_{scat}(\mathbf{r}_\perp, z_0, \omega) = k_0^2(\omega) \overset{\leftrightarrow}{\mathbf{G}}(\mathbf{r}_\perp, z, \omega) * \left[\mathbf{E}(\mathbf{r}_\perp, z, \omega) o(\mathbf{r}_\perp, z, \omega) \right] \quad (4)$$

where the convolution operator, $*$, is over the three spatial dimensions, (\mathbf{r}_\perp, z) . We apply a planar Fourier transform (P.F.T.) to Eqn. 4, to obtain,

$$\tilde{\mathbf{E}}_{scat}(\mathbf{k}_\perp, z_0, \omega) = \tilde{\mathcal{G}}(\mathbf{k}_\perp, z, \omega) \left[\tilde{\mathbf{E}}(\mathbf{k}_\perp, z, \omega) * \tilde{O}(\mathbf{k}_\perp, z, \omega) \right], \quad (5)$$

where the forward wave operator $\tilde{\mathcal{G}}$ is defined as

$$\tilde{\mathcal{G}}(\mathbf{k}_\perp, z, \omega) \left[\circ \right] \equiv k_0^2(\omega) \int_0^\infty dz' \overset{\leftrightarrow}{\mathbf{G}}(\mathbf{k}_\perp, z_0 - z', \omega) \cdot \left[\circ \right] \quad (6)$$

and the convolution operator, $*$, between the field $\tilde{\mathbf{E}}$ and the object \tilde{O} is over the two spatial frequency dimensions, \mathbf{k}_\perp .

In the planar Fourier transform domain, the wave operator and field terms partition naturally into propagating and evanescent components based upon whether $|\mathbf{k}_\perp|$ less than or equal to, or greater than $k_0(\omega)$, respectively. This is shown in Figure 1. In the next section, we use this to mathematically partition Eqn. 4 into propagating and evanescent components.

2.2. Partitioning the Spectra

Dropping the arguments for convenience, we partition the wave operator and field spectral terms of Eqn. 4 into the sum of propagating and evanescent spectral components as follows:

$$\tilde{\mathcal{G}} = \tilde{\mathcal{G}}_< + \tilde{\mathcal{G}}_>, \quad (7)$$

$$\tilde{\mathbf{E}}_{scat} = \tilde{\mathbf{E}}_{scat<} + \tilde{\mathbf{E}}_{scat>}, \quad (8)$$

$$\tilde{\mathbf{E}} = \tilde{\mathbf{E}}_< + \tilde{\mathbf{E}}_>, \quad (9)$$

where

$$\tilde{\mathcal{F}}_< \equiv \left\{ \tilde{\mathcal{F}}(\mathbf{k}_\perp, z, \omega) \mid |\mathbf{k}_\perp| \leq k_0(\omega) \right\}, \quad (10)$$

$$\tilde{\mathcal{F}}_> \equiv \left\{ \tilde{\mathcal{F}}(\mathbf{k}_\perp, z, \omega) \mid |\mathbf{k}_\perp| > k_0(\omega) \right\}. \quad (11)$$

That is the “<” and “>” subscripts indicate that $|\mathbf{k}_\perp|$ is less than or greater than the spectral cutoff of $k_0(\omega)$, respectively. Note: For any field term $\lim_{z \rightarrow \infty} \tilde{\mathcal{F}}_> = 0$, that is, the evanescent component vanishes as we move into the far-field.

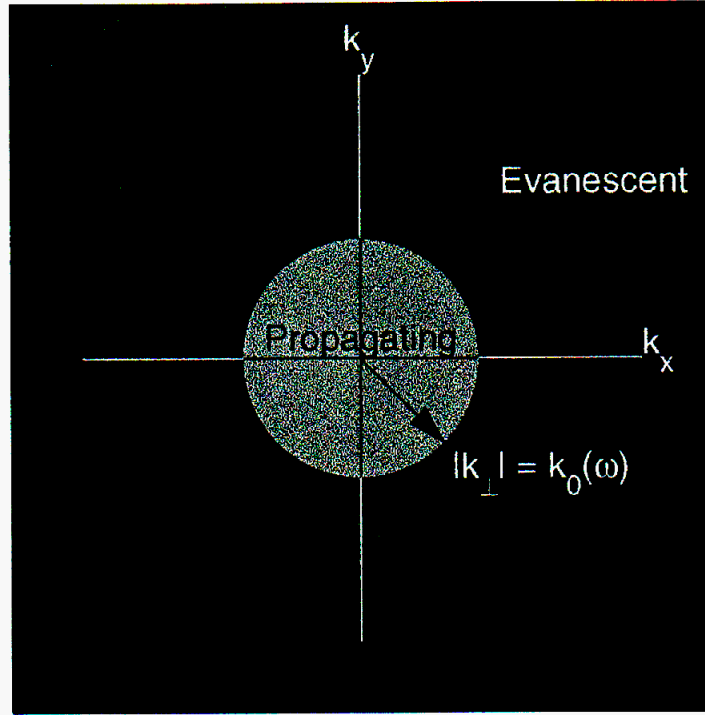


Figure 1. Planar Fourier transform domain partitioning of the wave operator and field spectral components.

The object, however, not being a field, does not have propagating and evanescent parts. It does have resolvable and non-resolvable parts depending upon the wavenumber cutoff of the field measurement system. Thus we write:

$$\tilde{O} = \underbrace{\tilde{O}_{<}}_{\text{resolvable}} + \underbrace{\tilde{O}_{>}}_{\text{non-resolvable}}. \quad (12)$$

Combining the partitioned terms, the Helmholtz equation of Eqn. 5,

$$\tilde{\mathbf{E}}_{\text{scat}} = \tilde{\mathcal{G}} [\tilde{\mathbf{E}} * \tilde{O}], \quad (13)$$

becomes:

$$\tilde{\mathbf{E}}_{\text{scat}<} + \tilde{\mathbf{E}}_{\text{scat}>} = (\tilde{\mathcal{G}}_{<} + \tilde{\mathcal{G}}_{>}) [(\tilde{\mathbf{E}}_{<} + \tilde{\mathbf{E}}_{>}) * (\tilde{O}_{<} + \tilde{O}_{>})]. \quad (14)$$

We further partition this into *far-field* and *near-field* terms using the

$$\lim_{z \rightarrow \infty} \tilde{\mathbf{F}}_{>} = 0$$

property of the field terms. This is shown in Figure 2. There are two physical effects occurring:

- A “smearing” of object spectral information due to the convolution with the field;
- A conversion between propagating and evanescent information via the wave operator.

Reconstruction algorithms which take these effects into account will result in imaging enhancements and superresolution. Most current techniques only consider the $\tilde{\mathcal{G}}_{<} [\tilde{\mathbf{E}}_{<} * \tilde{O}_{<}]$ term which is the sole surviving term of Eqn. 14 in the far-field. When operating in the near-field, however, these far-field algorithms would consider the evanescent terms as noise rather than as carrying useful information. There is a problem, however, in undoing the effects of the spectral convolution. The solution we propose in the next section is to beam-form the transmitted field so as to direct the probing energy into the object’s resolvable and non-resolvable components individually.

Far-Field ($z \rightarrow \infty$)

$$\begin{aligned}\tilde{\mathbf{E}}_{scat<} &= \tilde{g}_{<} \left[\tilde{\mathbf{E}}_{<} * \left(\tilde{O}_{<} + \tilde{O}_{>} \right) \right] \\ &= \underbrace{\tilde{g}_{<} \left[\tilde{\mathbf{E}}_{<} * \tilde{O}_{<} \right]}_{\text{current techniques}} + \underbrace{\tilde{g}_{<} \left[\tilde{\mathbf{E}}_{<} * \tilde{O}_{>} \right]}_{\text{currently treated as noise}}\end{aligned}$$

$$\tilde{\mathbf{E}}_{scat>} = 0$$

Near-Field

$$\tilde{\mathbf{E}}_{scat<} = \tilde{g}_{<} \left[\tilde{\mathbf{E}}_{<} * \left(\tilde{O}_{<} + \tilde{O}_{>} \right) \right] + \tilde{g}_{<} \left[\tilde{\mathbf{E}}_{>} * \left(\tilde{O}_{<} + \tilde{O}_{>} \right) \right]$$

$$\tilde{\mathbf{E}}_{scat>} = \underbrace{\tilde{g}_{>} \left[\tilde{\mathbf{E}}_{<} * \left(\tilde{O}_{<} + \tilde{O}_{>} \right) \right]}_{\text{currently ignored}} + \tilde{g}_{>} \left[\tilde{\mathbf{E}}_{>} * \left(\tilde{O}_{<} + \tilde{O}_{>} \right) \right]$$

Figure 2. Partitioning of the Helmholtz equation into near- and far-field terms with further partitioning into propagating and evanescent components.

3. BEAM-FORMING DEVELOPMENT OF GENERALIZED FOURIER DIFFRACTION THEOREM

In this section, we develop a method of separating the propagating and evanescent components of the received spectrum by beam-forming on transmit. The mathematical development follows that of Deming and Devaney.² We begin with the integral form of the Helmholtz equation,

$$\mathbf{E}_{scat}(\mathbf{r}_\perp, z_0, \omega) = k_0^2(\omega) \int d\mathbf{r}' \overset{\leftrightarrow}{\mathbf{G}}(\mathbf{r}_\perp - \mathbf{r}'_\perp, z_0 - z', \omega) \cdot \mathbf{E}(\mathbf{r}'_\perp, z', \omega) o(\mathbf{r}'_\perp, z', \omega), \quad (15)$$

where

$$o(\mathbf{r}_\perp, z, \omega) = \frac{\epsilon(\mathbf{r}_\perp, z, \omega)}{\epsilon_0} - 1, \quad (16)$$

$$\epsilon(\mathbf{r}_\perp, z, \omega) = \epsilon'(\mathbf{r}_\perp, z, \omega) + i \frac{\sigma(\mathbf{r}_\perp, z, \omega)}{\omega}, \quad (17)$$

$$\mu = \mu_0, \quad (18)$$

$$k_0(\omega) = \omega \sqrt{\epsilon_0 \mu_0}, \quad (19)$$

$$\mathbf{r} = \mathbf{r}_\perp + z\hat{z} = x\hat{x} + y\hat{y} + z\hat{z}. \quad (20)$$

The dyadic Green's function satisfies

$$[(\nabla \times \nabla \times) - k_0^2(\omega)] \overset{\leftrightarrow}{\mathbf{G}}(\mathbf{r}_\perp - \mathbf{r}'_\perp, z - z', \omega) = \overset{\leftrightarrow}{\mathbf{I}} \delta(\mathbf{r}_\perp - \mathbf{r}'_\perp) \delta(z - z'). \quad (21)$$

The solution to Eqn. 21 given in terms of its P.F.T. for $z < z'$ is¹:

$$\overset{\leftrightarrow}{\mathbf{G}}(\mathbf{r}_\perp - \mathbf{r}'_\perp, z - z', \omega) = \frac{i}{2(2\pi)^{n-1} k_0^2(\omega)} \int d\mathbf{k}_\perp \frac{1}{\gamma(\mathbf{k}_\perp, \omega)} \left[k_0^2(\omega) \overset{\leftrightarrow}{\mathbf{I}} + \mathbf{k}^+(\mathbf{k}_\perp, \omega) \mathbf{k}^+(\mathbf{k}_\perp, \omega) \right] \times e^{-i\mathbf{k}_\perp \cdot (\mathbf{r}_\perp - \mathbf{r}'_\perp)} e^{-i\gamma(\mathbf{k}_\perp, \omega)(z - z')} \quad (22)$$

where

$$n = 3 \text{ (dimensionality)}, \quad (23)$$

$$\mathbf{k}_\perp \equiv k_x \hat{x} + k_y \hat{y}, \quad (24)$$

$$\mathbf{k}^+(\mathbf{k}_\perp, \omega) \equiv \mathbf{k}_\perp + \gamma(\mathbf{k}_\perp, \omega) \hat{z}, \quad (25)$$

$$\gamma(\mathbf{k}_\perp, \omega) \equiv \sqrt{k_0^2(\omega) - |\mathbf{k}_\perp|^2}, \quad (26)$$

and the sign of Eqn. 26 is chosen so as to make $\text{Im}\{\gamma(\mathbf{k}_\perp, \omega)\} \geq 0$.

Substitute Eqn. 22 into Eqn. 15 and factor out $k_0^2(\omega)$

$$\mathbf{E}_{scat}(\mathbf{r}_\perp, z_0, \omega) = \frac{i}{2(2\pi)^{n-1}} \int d\mathbf{r}' \left[\int d\mathbf{k}_\perp \frac{1}{\gamma(\mathbf{k}_\perp, \omega)} \left[k_0^2(\omega) \overset{\leftrightarrow}{\mathbf{I}} + \mathbf{k}^+(\mathbf{k}_\perp, \omega) \mathbf{k}^+(\mathbf{k}_\perp, \omega) \right] \times e^{-i\mathbf{k}_\perp \cdot (\mathbf{r}_\perp - \mathbf{r}'_\perp)} e^{-i\gamma(\mathbf{k}_\perp, \omega)(z_0 - z')} \right] \cdot \mathbf{E}(\mathbf{r}'_\perp, z', \omega) o(\mathbf{r}'_\perp, z', \omega). \quad (27)$$

In order to simplify the notation, define $\overset{\leftrightarrow}{\mathbf{K}}(\mathbf{k}_\perp, \omega) \equiv \left[k_0^2(\omega) \overset{\leftrightarrow}{\mathbf{I}} + \mathbf{k}^+(\mathbf{k}_\perp, \omega) \mathbf{k}^+(\mathbf{k}_\perp, \omega) \right]$, and substitute it into Eqn. 27:

$$\mathbf{E}_{scat}(\mathbf{r}_\perp, z_0, \omega) = \frac{i}{2(2\pi)^{n-1}} \int d\mathbf{r}' \int d\mathbf{k}_\perp \frac{e^{-i\mathbf{k}_\perp \cdot (\mathbf{r}_\perp - \mathbf{r}'_\perp)} e^{-i\gamma(\mathbf{k}_\perp, \omega)(z_0 - z')}}{\gamma(\mathbf{k}_\perp, \omega)} \overset{\leftrightarrow}{\mathbf{K}}(\mathbf{k}_\perp, \omega) \cdot \mathbf{E}(\mathbf{r}'_\perp, z', \omega) o(\mathbf{r}'_\perp, z', \omega). \quad (28)$$

Interchanging the $d\mathbf{k}_\perp$ and $d\mathbf{r}'$ integrals,

$$\mathbf{E}_{scat}(\mathbf{r}_\perp, z_0, \omega) = \frac{i}{2(2\pi)^{n-1}} \int d\mathbf{k}_\perp \frac{e^{-i\mathbf{k}_\perp \cdot \mathbf{r}_\perp} e^{-i\gamma(\mathbf{k}_\perp, \omega)z_0}}{\gamma(\mathbf{k}_\perp, \omega)} \int d\mathbf{r}' \overset{\leftrightarrow}{\mathbf{K}}(\mathbf{k}_\perp, \omega) \cdot \mathbf{E}(\mathbf{r}'_\perp, z', \omega) e^{i\mathbf{k}_\perp \cdot \mathbf{r}'_\perp} e^{i\gamma(\mathbf{k}_\perp, \omega)z'} o(\mathbf{r}'_\perp, z', \omega), \quad (29)$$

and performing a planar Fourier transform,

$$\tilde{\mathbf{E}}_{scat}(\mathbf{k}'_{\perp}, z_0, \omega) = \int d\mathbf{r}_{\perp} \mathbf{E}_{scat}(\mathbf{r}_{\perp}, z_0, \omega) e^{i\mathbf{k}'_{\perp} \cdot \mathbf{r}_{\perp}}, \quad (30)$$

we obtain

$$\tilde{\mathbf{E}}_{scat}(\mathbf{k}_{\perp}, z_0, \omega) = \frac{ie^{-i\gamma(\mathbf{k}_{\perp}, \omega)z_0}}{2\gamma(\mathbf{k}_{\perp}, \omega)} \int d\mathbf{r}' \overset{\leftrightarrow}{\mathbf{K}}(\mathbf{k}_{\perp}, \omega) \cdot \mathbf{E}(\mathbf{r}'_{\perp}, z', \omega) o(\mathbf{r}'_{\perp}, z', \omega) e^{i\mathbf{k}_{\perp} \cdot \mathbf{r}'_{\perp}} e^{i\gamma(\mathbf{k}_{\perp}, \omega)z'}. \quad (31)$$

Using the plane-wave scattering matrix developed by Kerns,³ the measured scattered field is related to the measured voltage via the planar Fourier transform

$$u(\mathbf{r}_{\perp}, z_0, \omega) = \frac{1}{(2\pi)^{n-1}} \int d\mathbf{k}_{\perp} \mathbf{S}_{01}(\mathbf{k}_{\perp}, \omega) \cdot \tilde{\mathbf{E}}_{scat}(\mathbf{k}_{\perp}, z_0, \omega) e^{-i\mathbf{k}_{\perp} \cdot \mathbf{r}_{\perp}}, \quad (32)$$

where $\mathbf{S}_{01}(\mathbf{k}_{\perp}, \omega)$ describes the scattering characteristics of the receiving antenna. Inverse planar Fourier transforming, we have

$$U(\mathbf{k}_{\perp}, z_0, \omega) = \mathbf{S}_{01}(\mathbf{k}_{\perp}, \omega) \cdot \tilde{\mathbf{E}}_{scat}(\mathbf{k}_{\perp}, z_0, \omega). \quad (33)$$

Substituting Eqn. 31 into Eqn. 33, we find

$$U(\mathbf{k}_{\perp}, z_0, \omega) = \frac{ie^{-i\gamma(\mathbf{k}_{\perp}, \omega)z_0}}{2\gamma(\mathbf{k}_{\perp}, \omega)} \int d\mathbf{r}' \mathbf{S}_{01}(\mathbf{k}_{\perp}, \omega) \cdot \overset{\leftrightarrow}{\mathbf{K}}(\mathbf{k}_{\perp}, \omega) \cdot \mathbf{E}(\mathbf{r}'_{\perp}, z', \omega) o(\mathbf{r}'_{\perp}, z', \omega) e^{i\mathbf{k}_{\perp} \cdot \mathbf{r}'_{\perp}} e^{i\gamma(\mathbf{k}_{\perp}, \omega)z'}. \quad (34)$$

Before proceeding further, we invoke the Born approximation,^{1,4} and replace the unknown total field, $\mathbf{E}(\mathbf{r}'_{\perp}, z', \omega)$, within the integral with the known incident field, $\mathbf{E}_{inc}(\mathbf{r}'_{\perp}, z', \omega)$. We then express Eqn. 34 as

$$U^B(\mathbf{k}_{\perp}, z_0, \omega) = \frac{ie^{-i\gamma(\mathbf{k}_{\perp}, \omega)z_0}}{2\gamma(\mathbf{k}_{\perp}, \omega)} \int d\mathbf{r}' \mathbf{S}_{01}(\mathbf{k}_{\perp}, \omega) \cdot \overset{\leftrightarrow}{\mathbf{K}}(\mathbf{k}_{\perp}, \omega) \cdot \mathbf{E}_{inc}(\mathbf{r}'_{\perp}, z', \omega) o(\mathbf{r}'_{\perp}, z', \omega) e^{i\mathbf{k}_{\perp} \cdot \mathbf{r}'_{\perp}} e^{i\gamma(\mathbf{k}_{\perp}, \omega)z'}, \quad (35)$$

where the B superscript indicates we are operating under the Born approximation. In the forward model, we note the object is multiplied by the incident field. This multiplication in the spatial domain results in a convolution in the planar spectral domain, hence the "smearing" of the spectral components. The goal in the next section is to use a beam-formed incident field which can limit the effects of this smearing.

3.1. Development of the Transmitted Incident Field

Let incident field be produced by an array of N transmitters at locations $(\mathbf{r}_{\perp n}, z_s)$. Each transmitter produces a field given by^{2,3}

$$\mathbf{E}_{xmt}(\mathbf{r}_{\perp}, z, \omega) = \frac{C(\omega)}{(2\pi)^{n-1}} \int d\mathbf{k}'_{\perp} \mathbf{S}_{10}(\mathbf{k}'_{\perp}, \omega) e^{i\gamma(\mathbf{k}'_{\perp}, \omega)z} e^{-i\mathbf{k}'_{\perp} \cdot \mathbf{r}_{\perp}}, \quad (36)$$

where $C(\omega)$ is the time Fourier transform of the voltage wave form delivered to the antenna. The *total incident* field is given by beam-forming the fields from the individual transmitters:

$$\mathbf{E}_{inc}(\mathbf{r}'_{\perp}, z', \omega) = \frac{1}{N} \sum_{n=0}^{N-1} W(\mathbf{r}_{\perp n}, \omega) \mathbf{E}_{xmt}(\mathbf{r}'_{\perp} - \mathbf{r}_{\perp n}, z' - z_s, \omega) \quad (37)$$

$$= \frac{C(\omega)}{(2\pi)^{n-1}N} \sum_{n=0}^{N-1} W(\mathbf{r}_{\perp n}, \omega) \int d\mathbf{k}'_{\perp} \mathbf{S}_{10}(\mathbf{k}'_{\perp}, \omega) e^{i\gamma(\mathbf{k}'_{\perp}, \omega)(z' - z_s)} e^{-i\mathbf{k}'_{\perp} \cdot (\mathbf{r}'_{\perp} - \mathbf{r}_{\perp n})} \quad (38)$$

where the complex weight is defined as

$$W(\mathbf{r}_{\perp n}) \equiv w(\mathbf{r}_{\perp n})e^{i\omega\tau(\mathbf{r}_{\perp n})}, \quad (39)$$

with $w(\mathbf{r}_{\perp n})$ and $\tau(\mathbf{r}_{\perp n})$ real.

Substitute Eqn. 38 into Eqn. 35,

$$U^B(\mathbf{k}_\perp, z_0, \omega) = \frac{iC(\omega)e^{-i\gamma(\mathbf{k}_\perp, \omega)z_0}}{2(2\pi)^{n-1}N\gamma(\mathbf{k}_\perp, \omega)} \int d\mathbf{r}' \mathbf{S}_{01}(\mathbf{k}_\perp, \omega) \cdot \vec{\mathbf{K}}(\mathbf{k}_\perp, \omega) \cdot \left[\sum_{n=0}^{N-1} W(\mathbf{r}_{\perp n}, \omega) \int d\mathbf{k}'_\perp \mathbf{S}_{10}(\mathbf{k}'_\perp, \omega) e^{i\gamma(\mathbf{k}'_\perp, \omega)(z'-z_0)} e^{-i\mathbf{k}'_\perp \cdot (\mathbf{r}'_\perp - \mathbf{r}_{\perp n})} \right] \times o(\mathbf{r}'_\perp, z', \omega) e^{i\mathbf{k}_\perp \cdot \mathbf{r}'_\perp} e^{i\gamma(\mathbf{k}_\perp, \omega)z'}, \quad (40)$$

and interchange $d\mathbf{k}_\perp$ and $d\mathbf{r}'$ integrals

$$U^B(\mathbf{k}_\perp, z_0, \omega) = \frac{iC(\omega)e^{-i\gamma(\mathbf{k}_\perp, \omega)z_0}}{2(2\pi)^{n-1}\gamma(\mathbf{k}_\perp, \omega)} \int d\mathbf{k}'_\perp \mathbf{S}_{01}(\mathbf{k}_\perp, \omega) \cdot \vec{\mathbf{K}}(\mathbf{k}_\perp, \omega) \cdot \mathbf{S}_{10}(\mathbf{k}'_\perp, \omega) e^{-i\gamma(\mathbf{k}'_\perp, \omega)z_0} \times \left[\frac{1}{N} \sum_{n=0}^{N-1} W(\mathbf{r}_{\perp n}, \omega) e^{i\mathbf{k}'_\perp \cdot \mathbf{r}_{\perp n}} \right] \int d\mathbf{r}' o(\mathbf{r}'_\perp, z', \omega) e^{i(\mathbf{k}_\perp - \mathbf{k}'_\perp) \cdot \mathbf{r}'_\perp} e^{i(\gamma(\mathbf{k}_\perp, \omega) + \gamma(\mathbf{k}'_\perp, \omega))z'}. \quad (41)$$

In order to reduce the notation, we make the following definitions,

$$B(\mathbf{k}_\perp, \mathbf{k}'_\perp, \omega) \equiv \mathbf{S}_{01}(\mathbf{k}_\perp, \omega) \cdot \vec{\mathbf{K}}(\mathbf{k}_\perp, \omega) \cdot \mathbf{S}_{10}(\mathbf{k}'_\perp, \omega), \quad (42)$$

$$\Gamma(\mathbf{k}_\perp, \mathbf{k}'_\perp, \omega) \equiv \gamma(\mathbf{k}_\perp, \omega) + \gamma(\mathbf{k}'_\perp, \omega) \quad (43)$$

$$= \sqrt{k_0^2(\omega) - |\mathbf{k}_\perp|^2} + \sqrt{k_0^2(\omega) - |\mathbf{k}'_\perp|^2}, \quad (44)$$

$$\tilde{W}(\mathbf{k}'_\perp, \omega) \equiv \frac{1}{N} \sum_{n=0}^{N-1} W(\mathbf{r}_{\perp n}, \omega) e^{i\mathbf{k}'_\perp \cdot \mathbf{r}_{\perp n}}, \quad (45)$$

and substitute them into Eqn. 41. Then the planar Fourier transform of the measured scattered voltage of Eqn. 41 is expressed as

$$U^B(\mathbf{k}_\perp, z_0, \omega) = \frac{iC(\omega)e^{-i\gamma(\mathbf{k}_\perp, \omega)z_0}}{2(2\pi)^{n-1}\gamma(\mathbf{k}_\perp, \omega)} \int d\mathbf{k}'_\perp B(\mathbf{k}_\perp, \mathbf{k}'_\perp, \omega) e^{-i\gamma(\mathbf{k}'_\perp, \omega)z_0} \tilde{W}(\mathbf{k}'_\perp, \omega) \times \int d\mathbf{r}' o(\mathbf{r}'_\perp, z', \omega) e^{i(\mathbf{k}_\perp - \mathbf{k}'_\perp) \cdot \mathbf{r}'_\perp} e^{i\Gamma(\mathbf{k}_\perp, \mathbf{k}'_\perp, \omega)z'}. \quad (46)$$

Separate the $d\mathbf{r}'$ integral of Eqn. 46 into its $d\mathbf{r}'_\perp$ and dz' components,

$$U^B(\mathbf{k}_\perp, z_0, \omega) = \frac{iC(\omega)e^{-i\gamma(\mathbf{k}_\perp, \omega)z_0}}{2(2\pi)^{n-1}\gamma(\mathbf{k}_\perp, \omega)} \int d\mathbf{k}'_\perp B(\mathbf{k}_\perp, \mathbf{k}'_\perp, \omega) e^{-i\gamma(\mathbf{k}'_\perp, \omega)z_0} \tilde{W}(\mathbf{k}'_\perp, \omega) \int dz' e^{i\Gamma(\mathbf{k}_\perp, \mathbf{k}'_\perp, \omega)z'} \times \int d\mathbf{r}'_\perp o(\mathbf{r}'_\perp, z', \omega) e^{i(\mathbf{k}_\perp - \mathbf{k}'_\perp) \cdot \mathbf{r}'_\perp}, \quad (47)$$

and identify the $d\mathbf{r}'$ integral as being the planar Fourier transform of the object:

$$U^B(\mathbf{k}_\perp, z_0, \omega) = \frac{iC(\omega)e^{-i\gamma(\mathbf{k}_\perp, \omega)z_0}}{2(2\pi)^{n-1}\gamma(\mathbf{k}_\perp, \omega)} \int d\mathbf{k}'_\perp B(\mathbf{k}_\perp, \mathbf{k}'_\perp, \omega) e^{-i\gamma(\mathbf{k}'_\perp, \omega)z_0} \tilde{W}(\mathbf{k}'_\perp, \omega) \int dz' e^{i\Gamma(\mathbf{k}_\perp, \mathbf{k}'_\perp, \omega)z'} \times O(\mathbf{k}_\perp - \mathbf{k}'_\perp, z', \omega). \quad (48)$$

The result is the beam-formed Fourier Diffraction Theorem:

$$U^B(\mathbf{k}_\perp, z_0, \omega) = \frac{iC(\omega)e^{-i\gamma(\mathbf{k}_\perp, \omega)z_0}}{2(2\pi)^{n-1}\gamma(\mathbf{k}_\perp, \omega)} \int dz' \int d\mathbf{k}'_\perp O(\mathbf{k}_\perp - \mathbf{k}'_\perp, z', \omega) \times \tilde{W}(\mathbf{k}'_\perp, \omega) B(\mathbf{k}_\perp, \mathbf{k}'_\perp, \omega) e^{i\Gamma(\mathbf{k}_\perp, \mathbf{k}'_\perp, \omega)z'} e^{-i\gamma(\mathbf{k}'_\perp, \omega)z_0}. \quad (49)$$

We may now design transmitting array such that the spectrum of the weighting function, $\tilde{W}(\mathbf{k}_\perp, \omega)$, is identically zero for either $|\mathbf{k}_\perp| > k_0(\omega)$ or $|\mathbf{k}_\perp| \leq k_0(\omega)$, depending upon the spectral region we wish to probe. We note that for $\tilde{W}(\mathbf{k}_\perp, \omega) \equiv 1$, Eqn. 49 reduces to the case of a single monostatic transmitter.

Assuming we are now able to individually address the propagating and evanescent regions of the backscattered field, we consider in the next section the amount of energy scattered from each of the spectral regions.

4. EVANESCENT FIELD CONTENT

In order to quantify the evanescent portion of the backscattered field, we simulated and measured the field from a one-dimensional multi-monostatic scan of a small land mine shallowly buried in a sand box. The sandbox and exposed mine are shown in Figure 3. For the experiment, we scanned the buried mine with Lawrence Livermore National Laboratory's Micropower Impulse Radar⁵⁻⁷ (MIR).

If the received field is $u(x, z_0, t)$, its one-dimensional "planar" Fourier transform is given by

$$U(k_x, z_0, t) = \int dx u(x, z_0, t) e^{ik_x x}. \quad (50)$$

We further decompose $U(k_x, z_0, t)$ into its narrow band spectral components via a temporal Fourier transform:

$$\tilde{U}(k_x, z_0, \omega) = \int dt U(k_x, z_0, t) e^{i\omega t}. \quad (51)$$

We computed total power as

$$P_T(\omega) = \int dk_x \left| \tilde{U}(k_x, z_0, \omega) \right|^2, \quad (52)$$

the evanescent power via

$$P_e(\omega) = \int_{|k_x| > k_0(\omega)} dk_x \left| \tilde{U}(k_x, z_0, \omega) \right|^2, \quad (53)$$

and the percentage of evanescent power as

$$\%P_e(\omega) = 100 \frac{\int d\omega P_T(\omega)}{\int d\omega P_e(\omega)}. \quad (54)$$

Figure 4 shows the two-dimensional finite difference time domain (FDTD) simulation of the buried land mine. The top left plot shows the transmitted time series, a derivative of a Gaussian which approximates the actual transmitted MIR pulse. The top right plot shows the magnitude of the pulse spectrum. The graph in the lower left shows the computational domain with an overlay of the measurement plane which was 7.5 cm above the surface of the sand. The graph in the lower right shows the "measured" backscattered field, $u(x, z_0, t)$.

Figure 5 shows the P.F.T. results. The graph in the upper left shows the received field, $u(x, z_0, t)$. The graph in the upper right shows the narrow band decomposed P.F.T. of Eqn. 51. The wedge indicated by the two diagonal lines represent the $k_x = \pm k_0(\omega)$ cutoff. The graph at the bottom shows plots of the total power and evanescent power as a function of temporal frequency. We computed the evanescent power to be approximately 35% of the total backscattered power.

Figure 6 shows the measured results for the land mine and sandbox pictured in Figure 3. In this case, we found 28% of the returned power to be evanescent.

5. CONCLUSIONS

Most diffraction tomography reconstruction techniques assume far-field operation and justifiably ignore the evanescent fields. When operating in near-field conditions, the far-field algorithms would consider the evanescent fields as noise and reduce performance. We showed that incorporating the evanescent fields into the reconstruction algorithms is difficult due to the spectral smearing of the object and field spectra. To reduce this effect, we proposed a beam-forming approach to individually address the propagating and evanescent parts of the backscattered spectrum. Finally, using both a simulation and a laboratory experiment, we showed that when operating in a near-field environment, the evanescent power is approximately 28% of the returned power.

ACKNOWLEDGMENTS

We wish to thank Dr. Stephen Azevedo for his MIR support, Dr. Jeffrey Mast for the use of his FDTD code, and Patrick Welsh, Gregory Dallum, and Mark Vigars for letting us "mess" with their radar within their lab.

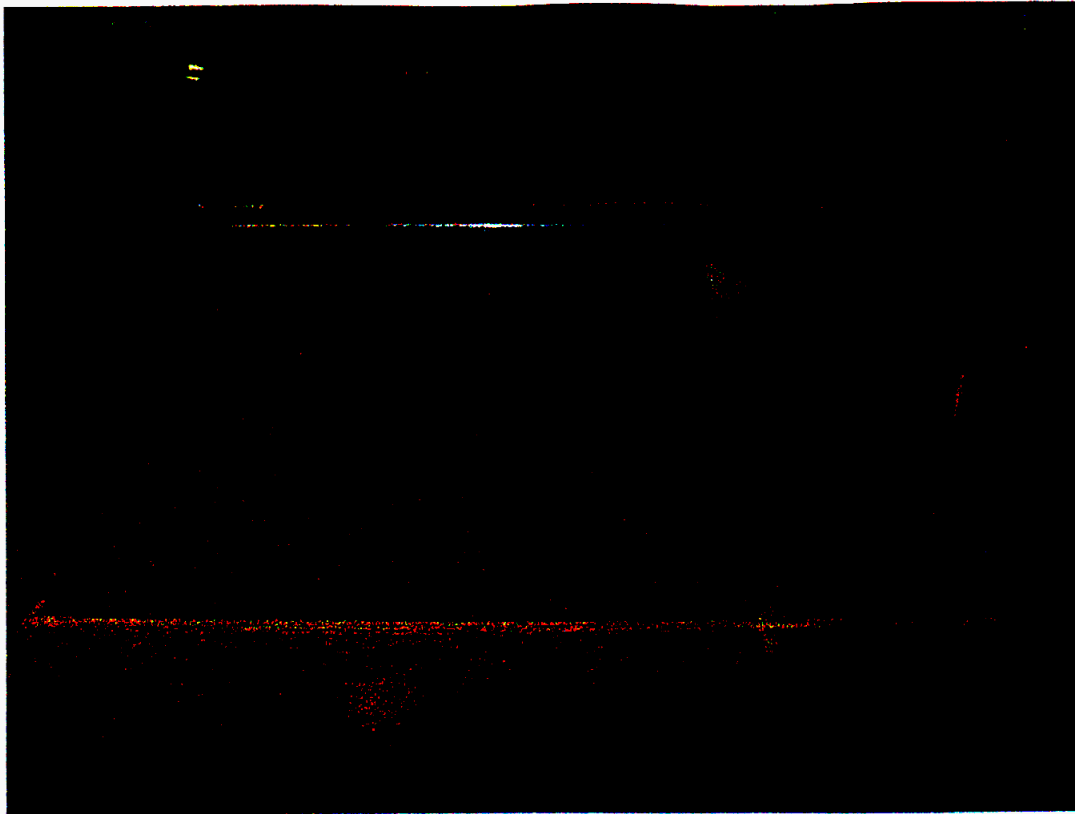


Figure 3. Sandbox and small land mine.

REFERENCES

1. W. C. Chew. *Waves and Fields in Inhomogeneous Media*. IEEE Press, 1995. ISBN 0-7803-1116-7.
2. R. W. Deming and A. J. Devaney. Diffraction tomography for multi-monostatic ground penetrating radar imaging. *Inverse Problems*, **13**:29–45, 1997.
3. D. M. Kerns. Plane-wave scattering-matrix theory of antennas and antenna-antenna interactions. Technical report, U. S. Dept. of Commerce, National Bureau of Standards, June 1981. NBS Monography 162.
4. K. J. Langenberg. Applied inverse problems for acoustic, electromagnetic and elastic wave scattering. In P. C. Sabatier, editor, *Basic Methods of Tomography and Inverse Problems*, Malvern Physics Series, chapter II. Adam Hilger, 1987. A set of lectures by G. T. Herman, H. K. Tuy, K. J. Langenberg, and P. C. Sabatier. ISBN 0-85274-285-1.
5. S. G. Azevedo and T. E. McEwan. Micropower impulse radar. *Science and Technology Review, Lawrence Livermore National Laboratory*, pages 16–29, 1996. UCRL-52000-96-1/2.
6. S. G. Azevedo, T. E. McEwan, and J. P. Warhus. Microradar development. *Engineering Research, Development and Technology: Thrust Area Report, Lawrence Livermore National Laboratory*, pages 6–17, 1996. UCRL-53868-95.
7. Lawrence Livermore National Laboratory. *MIR Technology Overview*, <http://lasers.llnl.gov/lasers/idp/mir/overview.html>.

This work was performed under the auspices of the U.S. Department of Energy by the University of California, Lawrence Livermore National Laboratory under Contract No. W-7405-Eng-48.

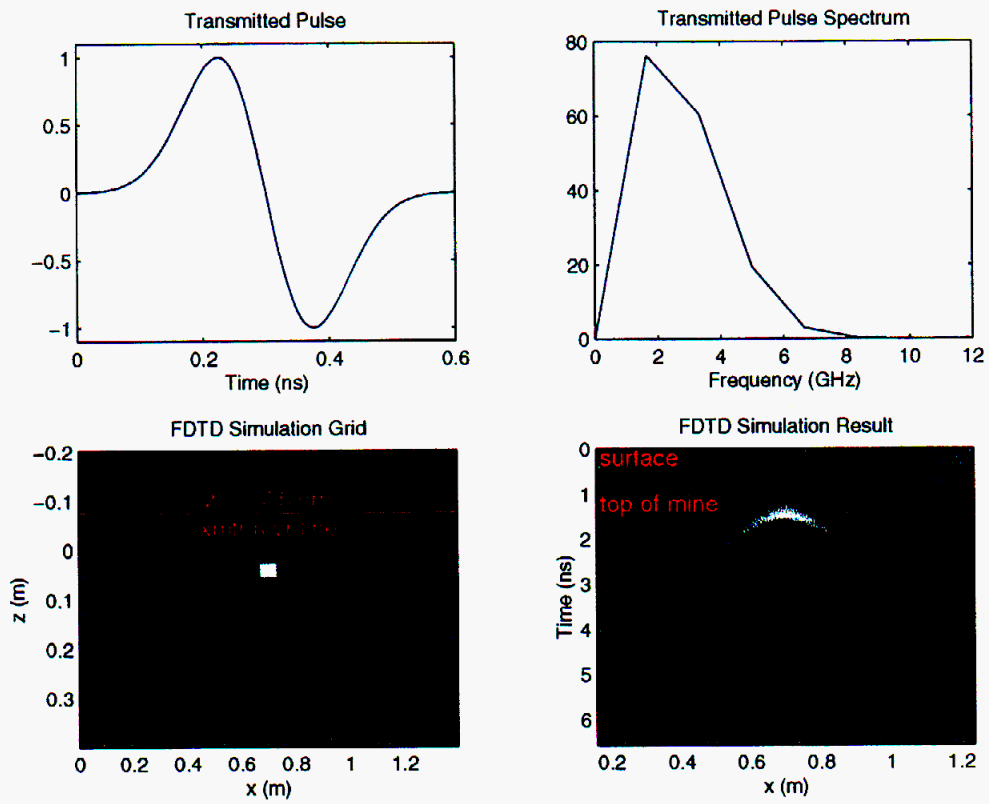


Figure 4. Simulated buried land mine.

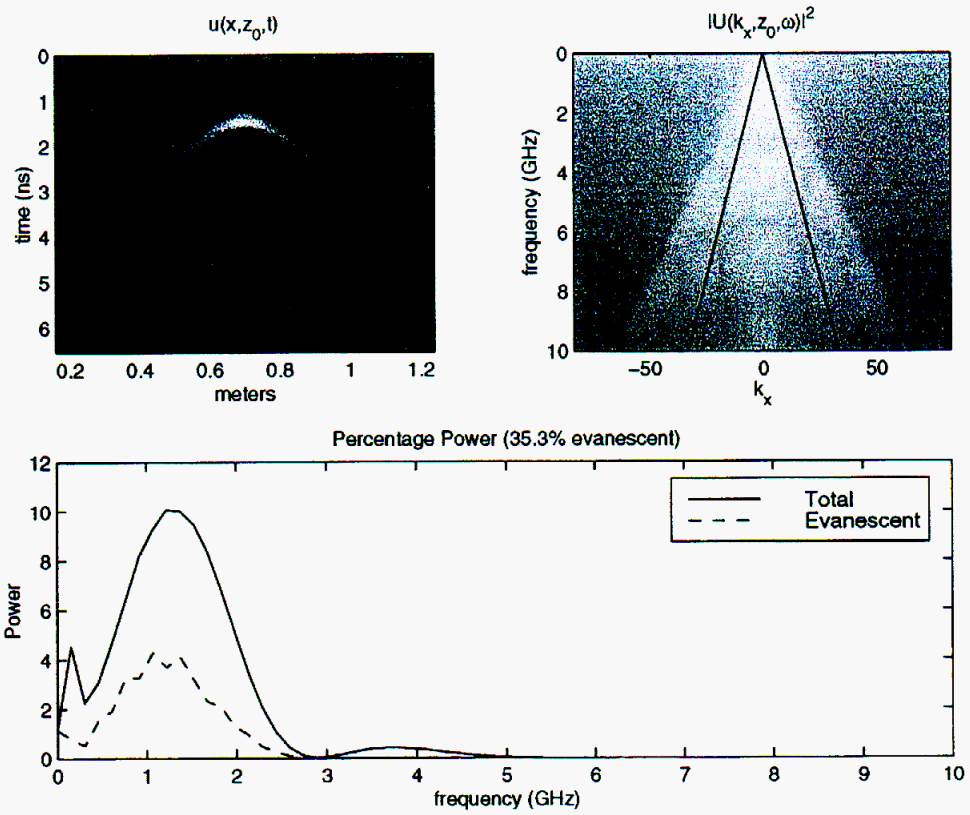


Figure 5. Evanescent power content of simulated buried land mine. 35% of the backscattered power is evanescent.

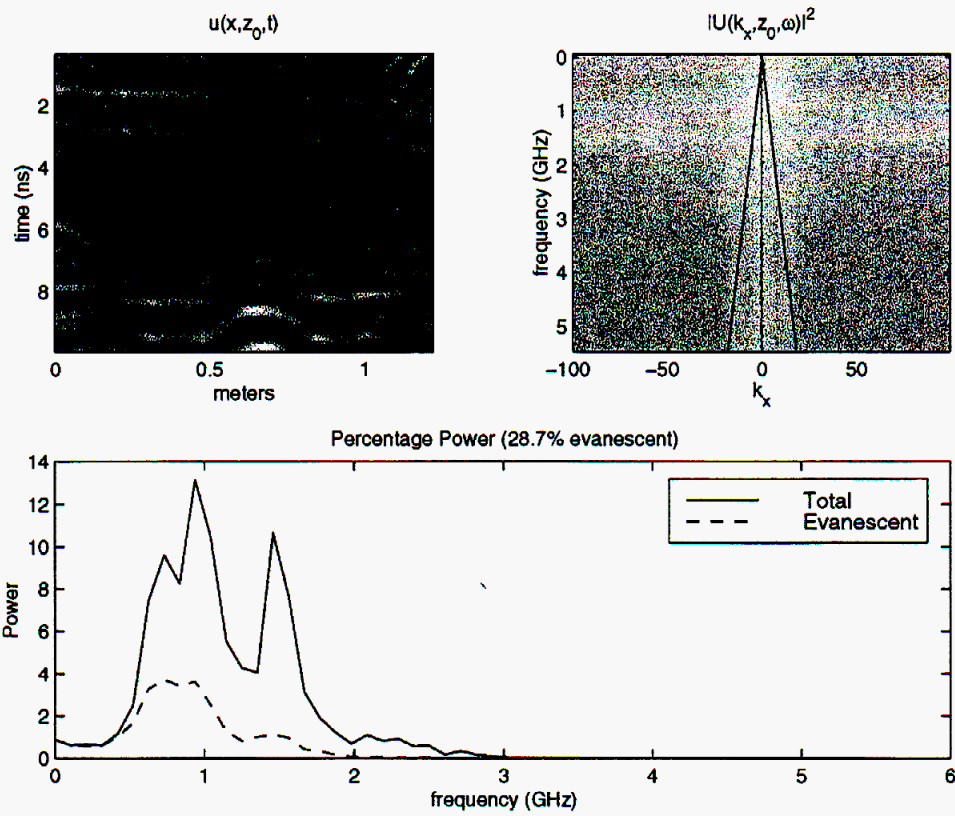


Figure 6. Evanescent power content of buried land mine. 28% of the backscattered power is evanescent.